CHEMIJA. 2019. Vol. 30. No. 4. P. 201–211

Comparative investigation of oxidative degradation of organic dye in the presence of H_2O_2 and CuO nanoparticles synthesized by sol–gel method and green synthesis using flower (*Matricaria chamomilla*) extract

D. Kaušpėdienė [1*],

E. Zubrytė [1],

A. Gefenienė [1, 2],

M. Jovaišaitė [2],

V. Gefenas [2],

R. Binkienė [1],

R. Ragauskas [1],

A. Selskienė [1],

V. Pakštas [1]

[1] Center for Physical Sciences and Technology, 3 Saulėtekio Avenue, 10257 Vilnius, Lithuania

[2] Vytautas Magnus University, 58 K. Donelaičio Street, 44248 Kaunas, Lithuania

In this study, CuO nanoparticles have been synthesized via a simple sol–gel method and green synthesis using flower (*Matricaria chamomilla*) extract. XRD analysis of the synthesized CuO nanoparticles clearly indicated a crystalline nature with a monoclinic structure regardless of the method of synthesis, while SEM revealed that the used synthesis methods affected the morphology of the CuO nanoparticles. The oxidative degradation kinetics of the organic dye Methyl Orange (MO) in the presence of the synthesized catalyst CuO and H_2O_2 has been investigated and compared depending on the dye concentration, reaction time and temperature. The catalytic activity of CuO was studied by measuring the UV–visible spectrum of the MO dye solution treated with CuO and H_2O_2. It was determined that the MO degradation reaction kinetics followed the pseudo-first-order mechanism. Thermodynamic studies indicated an endothermic nature ($\Delta H^{\#} = +73.03$ kJ mol^{-1}) and a decrease in randomness at the catalyst CuO/solution interface during the reaction ($\Delta S^{\#} = -0.021$ kJ mol^{-1} K^{-1}). At the same conditions, the green synthesized CuO nanoparticles exhibit similar activity properties as CuO synthesized using the sol–gel method. Besides, the green synthesis of CuO nanoparticles is simple and uses a small number of chemicals. The obtained CuO may be a promising catalyst for the oxidative degradation of organics, especially used in medical procedures.

Keywords: oxidative degradation of organics, catalyst CuO nanoparticles, sol–gel synthesis, green synthesis, Methyl Orange dye, kinetics

INTRODUCTION

The organic dyes are used in the dying industries such as textile as well as for dyeing anodized aluminum, in special analytical procedures including medical application. The inadequately treated industrial wastewater discharged into water bodies due to the dye toxicity and stability is a major hazard to the water environment [1]. This is related to the discharged coloured water and to the hazardous

* Corresponding author. Email: danute.kauspediene@ftmc.lt

carcinogenic properties of amines formed by reductive cleavage of azo groups of dyes and heavy metals, present in the metallized dye [2–4]. Therefore, to avoid their release into the environment and for water reuse in the industrial process, a complete removal of these hazardous dyes from wastewaters is necessary.

Many chemical and physical methods (coagulation, precipitation, filtration, membrane separation, electrodialysis, photochemical, oxidative degradation, biodegradation and adsorption) have been used for the removal of dyes from wastewaters [5]. It is now recognized that the advanced oxidation processes (AOPs) are the most effective technology for the degradation of various organic pollutants such as aromatic compounds, dyes, pharmaceutical compounds and pesticides present in industrial wastewater [6–8]. Moreover, AOPs are considered as highly competitive water treatment technology for the removal of chemically stable organic pollutants not treatable by conventional techniques due to their high chemical stability and low biodegradability. Usually AOPs include ozone oxidation, supercritical water oxidation, wet air oxidation, Fenton oxidation reaction (homogeneous and heterogeneous) and catalytic oxidation. Special attention is given to heterogeneous Fenton reactions which are highly efficient and generate no secondary pollution to the environment while saving energy [6–8].

In generally, AOPs result in the production of hydroxyl radicals (HO•) in the presence of a catalyst (metal or metal oxide nanoparticles), which oxidize organic pollutants to form CO_2, H_2O or some less toxic inorganic small molecules [9]. A variety of AOPs based on the generation of HO• have been established and classified based on the principal source of radicals: UV photolysis (direct and indirect), ozonation, electro-chemical treatment, ultrasound irradiation, non-thermal plasma, γ-ray and electron beam irradiation. Whereas catalytic iron species constituting metal salts (in Fe^{2+} or Fe^{3+} form), metal oxides (e.g. Fe_2O_3, Fe_3O_4) and zero-valent metal (Fe^0) have been used for chemical (classical Fenton), photochemical (photo-Fenton) and electrochemical (electro-Fenton) degradation methods. These methods operate in strict acidic conditions to prevent iron precipitation. The elements with multiple redox states (like chromium, cerium, copper, cobalt, manganese and ruthenium) have also been suggested for hydrogen peroxide (H_2O_2) activation in neutral/alkaline conditions in both homogeneous and heterogeneous reaction conditions (non-iron Fenton catalysts methods) [10]. Copper, both monovalent (Cu^+) and divalent (Cu^{2+}), shows strikingly similar redox properties to iron as monovalent (Cu^+) and divalent (Cu^{2+}) oxidation states react easily with H_2O_2 by analogy with the Fe^{2+}/H_2O_2 and Fe^{3+}/H_2O_2 reaction systems. The hydrolyzed complexes with the most stable oxidation state, i.e. $Cu(OH)_2$ for Cu^{2+} and $FeOH(H_2O)^{2+}$ for Fe^{3+}, are both Fenton-active catalysts [11]. However, the iron aqua complex $[Fe(H_2O)_6]^{3+}$ is insoluble at pH > 5, while the corresponding copper complex $[Cu(H_2O)_6]^{2+}$ is predominant in neutral pH conditions [12]. This means that the Cu^{2+}-based Fenton catalysts efficiently generate HO• for the oxidation of various organic pollutants in near-neutral or neutral aqueous solutions. Hydrogen peroxide is the simplest oxidant that can easily generate HO• radicals on self-decomposition over the CuO catalyst by forming a Cu^{2+}/Cu^+ couple. Without doubt, the CuO nanostructures can be used as catalysts in neutral wastewater treatment practice [5].

Copper oxide nanoparticles characterized by unique physical and chemical properties are widely applicable not only in heterogeneous organic catalysis, sensing, superconductors, lithium ion electrode materials, different fields of solar energy cells and various medical applications, but also in catalytic degradation of organic water pollutants [13–21]. Either way, the CuO has presented a high catalytic activity, being attributed to morphological and superficial aspects.

Copper nanostructures were evaluated for the discolouration of cationic and anionic dye (Acid Fuchsin Dye, Rhodamine B, Methylene Blue, Methyl Orange, Bromothymol Blue (BTB), Methylene Blue, Congo Red and Remazol Golden Yellow) [5, 22–26].

Chemical and physical methods that are employed for the synthesis of Cu/CuO nanoparticles include polymer-assisted hydrothermal synthesis, microwave-assisted hydrothermal synthesis, electrochemical, surfactant-assisted coprecipitation, anodization of a chemically etched copper substrate and template free hydrothermal sol–gel synthesis. They remain expensive and involve the use of hazardous reagents as sodium citrate,

sodium borohydride and acids, NH_4OH, NaOH, urea and alcohols that are responsible for biological risks [26–32].

The 'green synthesis' (biological synthesis, eco-friendly synthesis) using plant extracts, among physical and chemical synthesis methods, has been used to synthesize Cu/CuO because it is greener, energy-saving and more cost-effective [33, 34]. Plant extracts have been proven to possess high efficiency as stabilizing and reducing agents for the synthesis of controlled shapes, sizes, structures and other specific features of metal and metal oxide nanoparticles. Plants are widespread, readily available and safer, and act as a source of many metabolites. Plant extracts contain phytochemicals, such as carbohydrates and proteins, which serve as a reducing agent for the reduction of metal ions and facilitate the formation of metal nanoparticles. Functional groups such as –C–O–C–, –C–O–, –C=C– and –C=O– derived from alkaloids, flavones and anthracenes are involved in the synthesis of metal nanoparticles [34–36]. It has been suggested that flavonoids (quercetin, dihydroquercetic, rutin and morin) may play a significant role in the formation of silver nanoparticles by reduction in the green synthesis of AgNP [37]. The plant phytochemicals also were responsible for the formation of metal oxide nanoparticles when oxygen either from the atmosphere or from the degrading phytochemical will bind the formerly reduced metal ions. Metal oxide ions will bind to each other due to electrostatic attraction and form into nanoparticles. The nanoparticles formed are then stabilized by certain phytochemicals to avoid agglomeration between them.

Various plant extracts have been used for the synthesis of CuO nanoparticles [25, 38–44]. *Rosa canina* fruit extract as a stabilizing and reducing agent for the synthesis of CuO nanoparticles has been employed. These obtained nanoparticles were used as an appropriate nanocatalyst for N-arylation of indole, aniline and benzyl amine via Ullmann-type C–N coupling reactions [38]. Using an aqueous extract of *Thymus vulgaris* L. leaves as a reducing and capping agent, copper oxide (CuO) nanoparticles were synthesized by the biological method. Importantly, synthesized CuO nanoparticles were found to be an excellent heterogeneous catalyst for ligand-free N-arylation of indoles and amines [39].

The leaf extract of *Impatiens balsamina* has been used in preparing from the copper sulphate solution CuO nanoparticles that are photocatalytic active in the degradation of the textile dye Methylene Blue and Congo Red under solar irradiation and capable for instant mercury detection [25]. The *Cordia sebestena* flower aqueous extract has also been used for the synthesis of CuO nanoparticles [40]. It was determined that the flower extract contains active phytoconstituents like phenol, flavonoid, tannin, phytosterol, coumarin, fumaric acid and atocopherol that are involved in synthesis. The nanoparticles were evaluated for their catalytic efficiency in degradation of Bromothymol Blue by photocatalysis with hydrogen peroxide. 100% removal efficiency of the Bromothymol Blue dye was achieved by 3 h exposure to natural sunlight inferring it as an economical, eco-friendly and effective catalyst. The biological significance of the green synthesized CuO nanoparticles was assessed by antibacterial activity against the selected pathogenic bacterial organisms [40]. The highly stable copper oxide nanoparticles, with an average size of about 14 nm, have been synthesized for medical applications using copper chloride dihydrate and sodium hydroxide in the presence of *Malva sylvestris* leaf extract at 80°C [41]. CuO nanoparticles with optical properties have been synthesized using *Aloe vera* leaf extract and copper sulphate solution. Nanoparticles showed a particle size of 20 nm. It was determined that the flavonoids, proteins and other functional groups present in the *Aloe vera* leaf extract can be responsible for the formation of copper oxide nanoparticles [42]. The morphology of the copper oxide nanoparticles was determined by the amount of *Aloe vera* extract. It was noted that this eco-friendly approach of synthesis is a novel, cheap and convenient technique suitable for large scale commercial production and health-related applications of CuO nanoparticles. *Andean blackberry* fruit and leaf extracts have been applied for the nontoxic/biodegradable synthesis of CuO nanoparticles due to the encapsulation of phytochemicals [43]. The improved antioxidant effectiveness of CuO nanoparticles synthesized using the fruit and leaf extract against 0.1 mM 1,1-diphenyl-2-picrylhydrazyl was obtained as 89.02 and 75.92%, respectively.

A simple and efficient synthesis method of catalytically active CuO nanoparticles was proposed

using *Anthemis nobilis* L. flower extract as a reducing and stabilizing agent without application of toxic reagents or a surfactant template [44]. It has been shown that the synthesized catalytically active CuO nanoparticles can be employed in catalyzing the aldehyde–amine–alkyne coupling reaction. The catalyst can be easily separated from the reaction mixture by a simple centrifugation and reused without further disposal.

The synthesis of CuO nanoparticles using the medicinal plant *Matricaria recutita* (*German chamomilla*) flower extract as both reducing and capping agent has been investigated [45]. The interaction with plasmid DNA (pBR322) was studied. It has been proven that the antioxidant activity and DNA cleavage properties of synthesized CuO nanoparticles depended on CuO concentration [45].

The genus *Anthemis nobilis* L. (Roman chamomile, German chamomile) belongs to the family Asteraceae (Compositae), is a multi-branched aromatic annual herb that spreads quickly to northern Europe and West Asia and also is one of important medicinal herbs cultivated in the world. Chamomile flower extract consists of flavonoids such as catechin, kaempferol and quercetin that were identified and determined using capillary electrophoresis with diode array detection (CE-DAD) [46].

Owing to scare publications concerning the oxidative degradation of the Methyl Orange (MO) dye in the iron-free Fenton-like system, this research describes the synthesis of catalyst CuO nanoparticles and their use. The catalytic activity properties of CuO prepared by the sol–gel method and an eco-friendly, green synthesis method using the *Matricaria recutita* (chamomile) flower extract were examined and compared. The kinetics and thermodynamics of the MO oxidative degradation reaction were studied. The structure and morphology of the catalyst CuO nanoparticles were characterized by XRD and SEM, while the catalytic activity was studied by measuring the UV–visible spectra of the MO dye solution treated by CuO/H_2O_2.

2. EXPERIMENTAL

Materials

Analytical grade copper sulphate ($CuSO_4 \cdot 5H_2O$), copper nitrate ($Cu(NO_3)_2\ 3H_2O$), sodium hydroxide (NaOH), hydrochloric acid (HCl), citric acid and H_2O_2 (35 wt%) were supplied from Thermo-Fisher GmbH (Alfa Aesar, Germany). Methyl Orange (MO) dye was obtained from Sigma-Aldrich Chemie GmbH, Germany (Fig. 1).

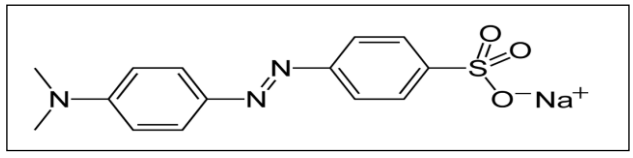

Fig. 1. Structure of Methyl Orange (empirical formula $C_{14}H_{14}N_3NaO_3S$; molecular weight 327.33)

Matricaria recutita (chamomile) crushed flowers were obtained from A. Karvelis Therapy-Phytotherapy Company (Lithuania). Deionized water was used to carry out all wet experiments.

Preparation of chamomile extract

10 g of dried crushed chamomile flowers was refluxed at 70°C with 200 mL of distilled water for 5 min. Then the mixture was allowed to cool to room temperature and an aqueous extract was easily obtained by filtration.

Preparation of CuO nanoparticles by sol–gel method [32]

CuO nanoparticles were synthesized by adding 0.2 mL portions of 1 M NaOH solution to a 200 mL mixture of 0.1 M $CuSO_4$ and 0.1 M citric acid solution with vigorous stirring to pH ≥ 12 (Fig. 2) when the $Cu(OH)_2$ precipitate was formed.

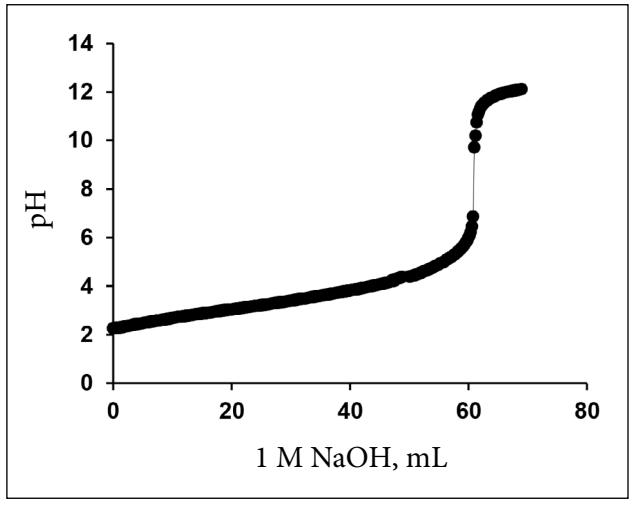

Fig. 2. The solution pH variation during the formation of the precursor for CuO nanoparticles synthesis using sol–gel method

The precipitate obtained was washed 3 times with 40 mL deionized water to remove possible by-ions present in the final products and dried. The obtained product was kept at 500°C for 3 h in a muffle furnace to get the final product of CuO nanoparticles.

Green synthesis of CuO nanoparticles [45]

200 mL of the aqueous extract of chamomile flowers was added dropwise to 50 mL of a well-mixed 0.003 M aqueous solution of $Cu(NO_3)_2$ with constant stirring at 40°C. After 5 min the colour of the solution was changed during the heating process that indicates the formation of CuO nanoparticles. The obtained solution of CuO nanoparticles was centrifuged at 6500 rpm for 30 min, washed 3 times with deionized water, and the precipitation was then air dried for 24 h at room temperature. The obtained product was calcined in a muffle furnace for 1 h at 800°C temperature.

CuO characterization

The surface morphology of the CuO nanoparticles was studied by using a scanning electron microscope EVO 50EP (Carl Zeiss SMT AG) equipped with energy and wave dispersive X-ray spectrometers (Oxford Instruments) and a secondary electron detector (low vacuum mode, 10 kV, 50 Pa, working distance 10 mm).

X-ray powder diffraction (XRD) data were measured with an X-ray diffractometer SmartLab (Rigaku, Japan), equipped with a 9 kW rotating Cu anode X-ray tube, using the Bragg–Brentano geometry with a graphite monochromator on the diffracted beam and a step scan mode with a step size of 0.02° (in 2θ scale) and counting time of 1 s per step. The measurements were conducted in a 2θ range of 10°–70°. Phase identification was performed using the software package PDXL (Rigaku) and ICDD powder diffraction data-base PDF-4+ (2013 release).

Catalytic experiments

The dye Methyl Orange (MO) was chosen to investigate the catalytic activity of the CuO nanostructures synthesized by sol–gel or green synthesis methods. To the 10 mL aqueous solution of the dye (5 or 10 mg/L) of 50°C or 25°C temperature 1 mL of H_2O_2 (35 wt%) was added. Immediately, 3 mg of the catalyst was added and as the reaction proceeded, the colour of the solution faded. The entire mixture was stirred during the reaction period. The supernatant was then transferred to a quartz cuvette for UV–visible spectral measurement. After the spectrum was measured, the solution was transferred back to the previous reaction vessel while stirring. The process was repeated and UV–visible spectra were recorded consecutively, to check the progress of the reaction. Blank experiments were also conducted to confirm that the reactions did not proceed with a catalyst in the absence of H_2O_2, or without a catalyst in the presence of H_2O_2.

UV–visible spectra were measured using a Varian Cary 50 spectrometer from Agilent Technologies (USA).

RESULTS AND DISCUSSION

Characterization of synthesized CuO

Figure 3 presents the XRD patterns of CuO synthesized by the sol–gel method (Fig. 3a, a red line) and by green synthesis using the extract of chamomille flowers (Fig. 3b, a black line) in comparison with the CuO standards (tenorite, Card No. 04-007-0518 (Fig. 3a, a green line) for sol–gel method and tenorite, Card No. 04-008-8209 (Fig. 3b, a green line) for green synthesis). The diffraction peaks indicate the same to the tenorite position of the CuO synthesized by both methods. The lattice parameters of the CuO networks are well synchronized to the lattice parameters of the standard tenorite (Table 1) which clearly indicates that the obtained CuO nanoparticles are of a crystalline nature with a monoclinic structure regardless of the method of synthesis. That observation correlates with previous reports about CuO nanoparticles synthesized by the hydrothermal method [5, 24], microwave hydrothermal method [26] and by green synthesis using *Cordia sebestena* [40].

Scanning electron microscopy was used to measure the difference in the morphology of CuO depending on the synthesis method. The SEM images of the CuO samples presented in Fig. 4a, b show that the synthesis method affected the morphology of the obtained CuO nanoparticles. CuO synthesized using the sol–gel method has the same smaller nearly spherical nanocrystallites about 70 nm in diameter and interconnected ultrafine

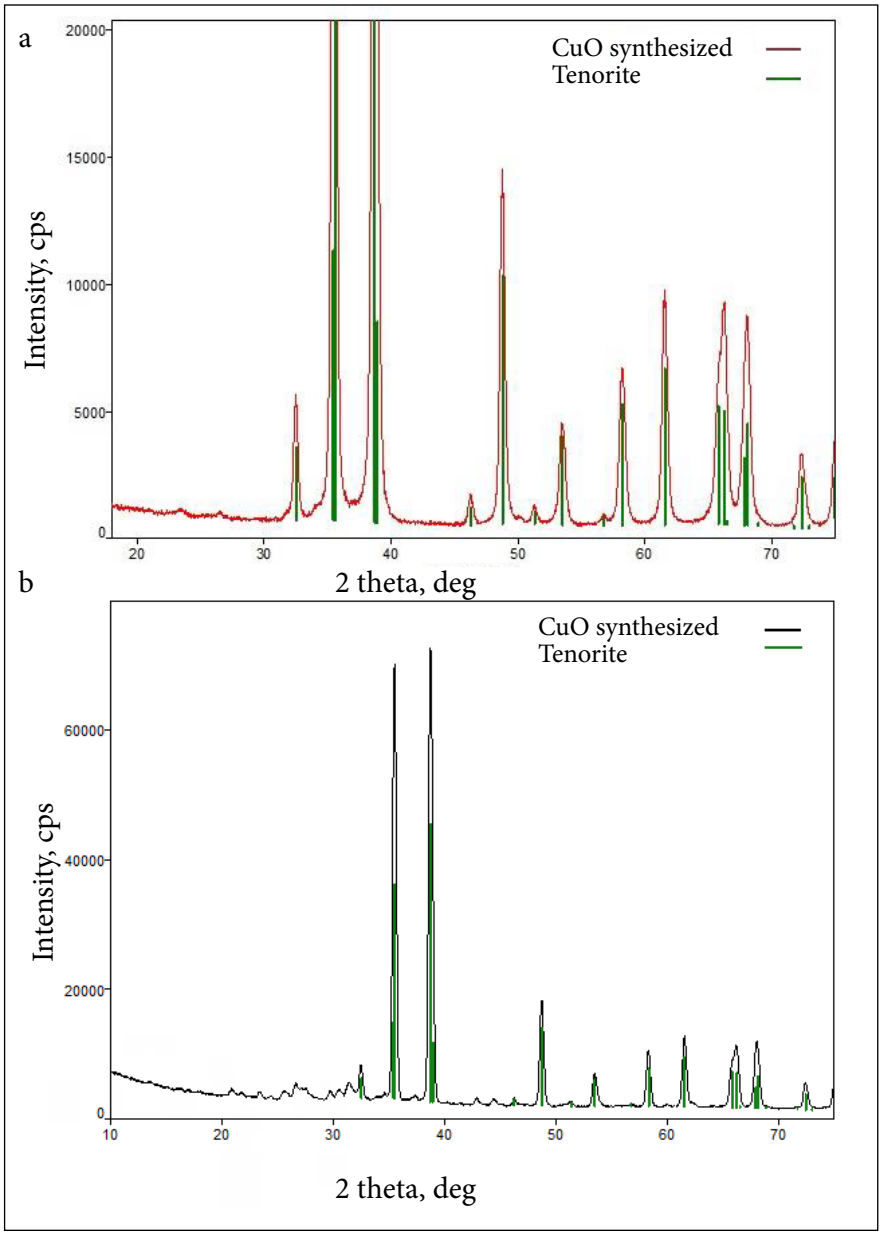

Fig. 3. XRD patterns of CuO synthesized by two different methods: (a) sol–gel method; (b) green synthesis

Table 1. **Lattice parameters (a, b, c, β) and the unit cell volume (V) of CuO samples synthesized by sol–gel and by green synthesis methods**

Sample	Lattice parameters (Å)				V (Å^3)
	a	b	c	β	
CuO standard (tenorite)	4.6837	3.4226	5.1288	99.54	81.20
CuO (sol–gel)	4.6833	3.4208	5.1294	99.57	81.03
CuO green synthesis	4.6851	3.4232	5.1311	99.39	81.19

particles with nano dimensions forming agglomerates, while the CuO particles obtained by green synthesis have the the same irregular rectangle-like blocks about 70–140 nm in diameter and sticks form particles of a similar diameter but 200–400 nm in length.

To compare the catalytic performance of the CuO nanoparticles synthesized by the sol–gel method

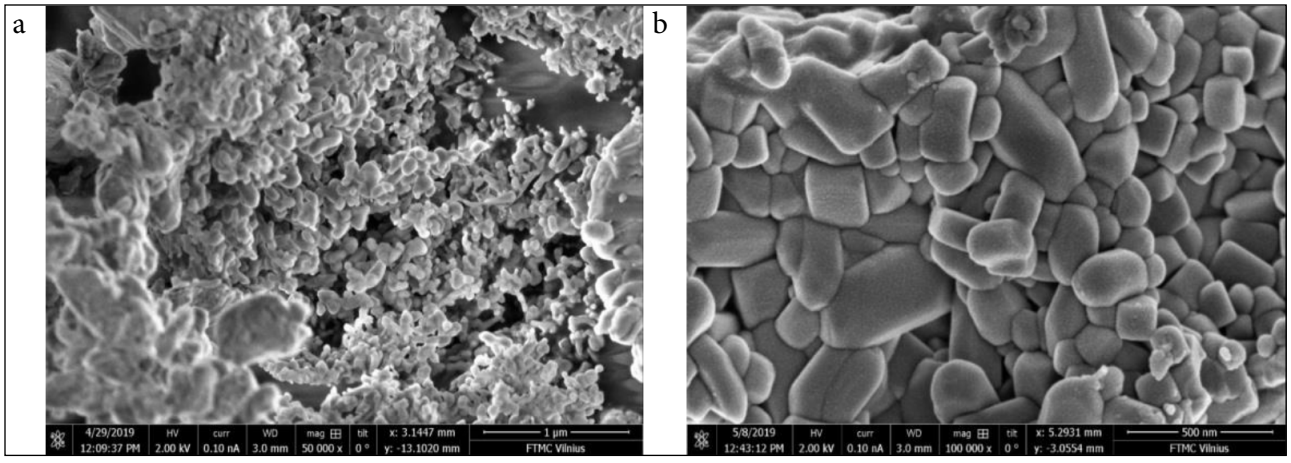

Fig. 4. Images obtained by SEM for CuO synthesized by two methods: (a) sol–gel method, magnitude 50 000 times; (b) green synthesis, magnitude 100 000 times

and green synthesis, the oxidative degradation of the organic dye Methyl Orange (MO) in the presence of H_2O_2 was investigated at pH varied from pH = 4.5 to pH = 6.5 and temperature from 25°C to 50°C.

It is known that in an aqueous solution, the CuO surface is covered with –OH functional groups formed by dissociative chemisorption of water molecules and that it is like a Bronsted–Lowry base behaving as a proton acceptor. These protons are in the form of a hydrogen (H^+) ion [24]

$$CuOH + H_2O \leftrightarrow CuOH^{2+} + HO^-. \quad (1)$$

Thus MO dye anions (RSO_3^-) are electrostatically attracted on the positive catalyst surface (physical adsorption), where the dye degradation process in the presence of H_2O_2 occurs. There is strong evidence that CuO shows similar redox properties like iron [5, 24, 47]. Both the divalent (Cu^{2+}, Eq. 2) and monovalent (Cu^+, Eq. 3) oxidation states react easily with H_2O_2 like the Fe^{2+}/H_2O_2 and Fe^{3+}/H_2O_2 reaction systems, respectively [47]:

$$Cu(II) + H_2O_2 \rightarrow Cu(I) + HO_2\bullet + H^+, \quad (2)$$

$$Cu(I) + H_2O_2 \rightarrow Cu(II) + HO\bullet + HO^-, \quad (3)$$

$$2Cu(I) + O_2 + 2H^+ \rightarrow 2Cu(II) + H_2O_2. \quad (4)$$

The UV–visible absorption spectra of 5 mg/L MO dye solution degradation at 50°C temperature using the CuO catalysts synthesized by two different methods (sol–gel and green synthesis) are presented in Fig. 5a, d, respectively. The spectrum of MO before adding H_2O_2 and CuO shows two characteristic peaks at 270 nm and 460 nm. As the degradation reaction proceeded, the characteristic peaks at 460 nm gradually tumbled when the reaction time increased. The higher solution temperature is favourable for MO dye degradation (Fig. 5a, b). This is clearly reflected in the calculated values of the degradation rates.

Based on the UV-absorbance data at a wavelength of 460 nm, presented in Fig. 6, MO degradation rates were calculated according to Eq. 5, and the obtained values are presented in Fig. 7:

$$\text{Degradation rate, \%} = \frac{(A_0 - A)}{A_0} \times 100. \quad (5)$$

Here A_0 is the absorbance at the initial time $t = 0$; A is the absorbance at the degradation reaction time t.

From Figs. 5, 6 and 7 it was observed that the degradation of MO using CuO synthesized by both sol–gel method and green synthesis is rapid from the initial stage until the maximum MO degradation rate is attained. That is possible due to diminishing nondegraded dye concentration in the solution and the release of CuO active centers according to Eqs. 2 and 3. Besides, the degradation rate decreases with the initial MO concentrations and temperature decrease. On the other hand, the increase of the degradation rate of MO with the increase in temperature indicates not only the mobility of the dye molecule but also the rate of the degradation reaction. It is notable that the

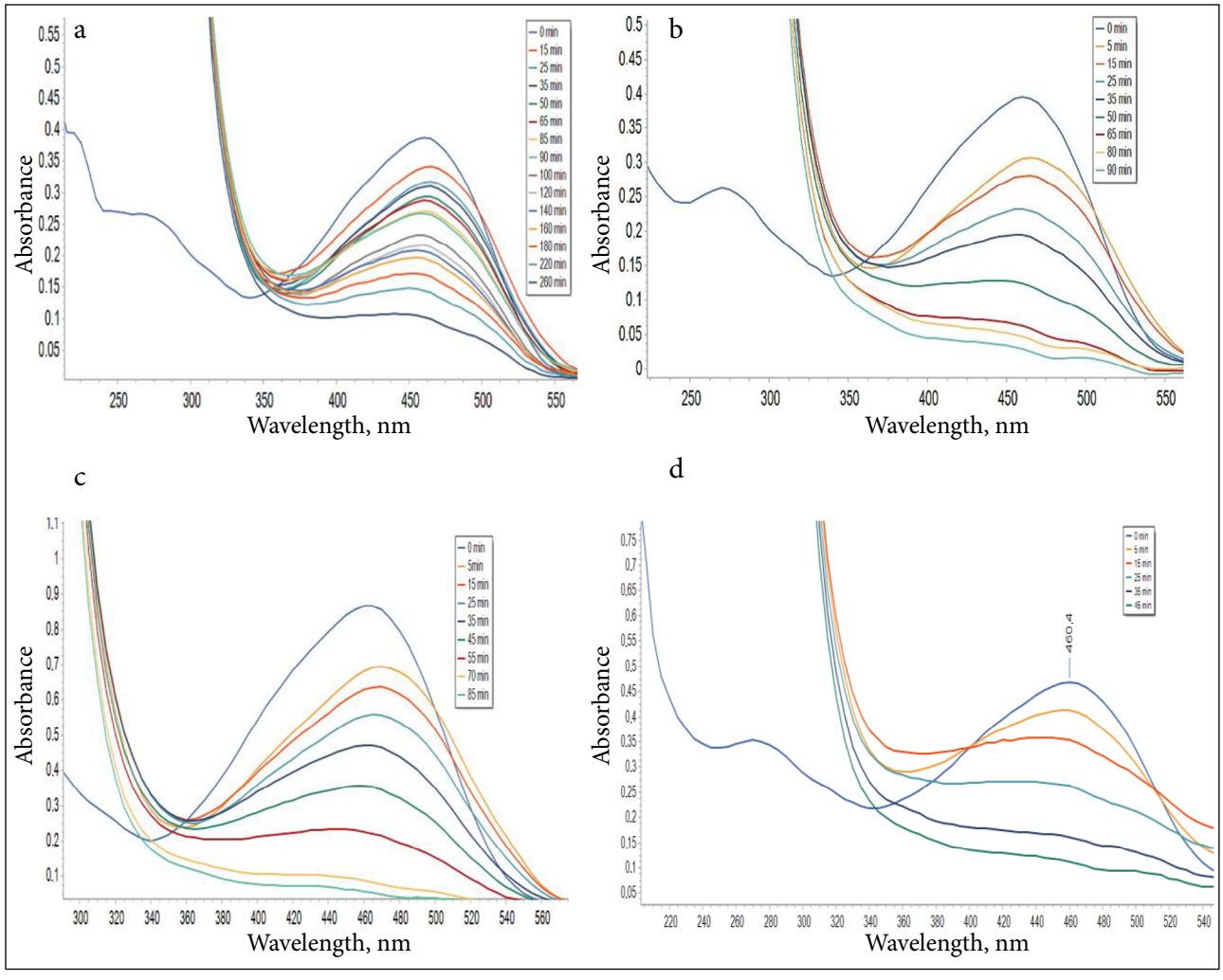

Fig. 5. Time dependent UV–vis absorbance of the MO before and during the degradation reaction of MO mixtures with H_2O_2 and catalyst CuO: (a) 5 mg/L MO, $T = 25$°C, CuO synthesized by sol–gel method; (b) 5 mg/L MO, $T = 50$°C, CuO synthesized by sol–gel method; (c) 10 mg/L MO, $T = 50$°C, CuO syntesized by sol–gel method; (d) 5 mg/L MO, $T = 50$°C, green synthesized CuO

Conditions: 10 mL MO solution (concentration MO 5 mg/L or 10 mg/L), 1 mL H_2O_2, catalyst 3 mg CuO.

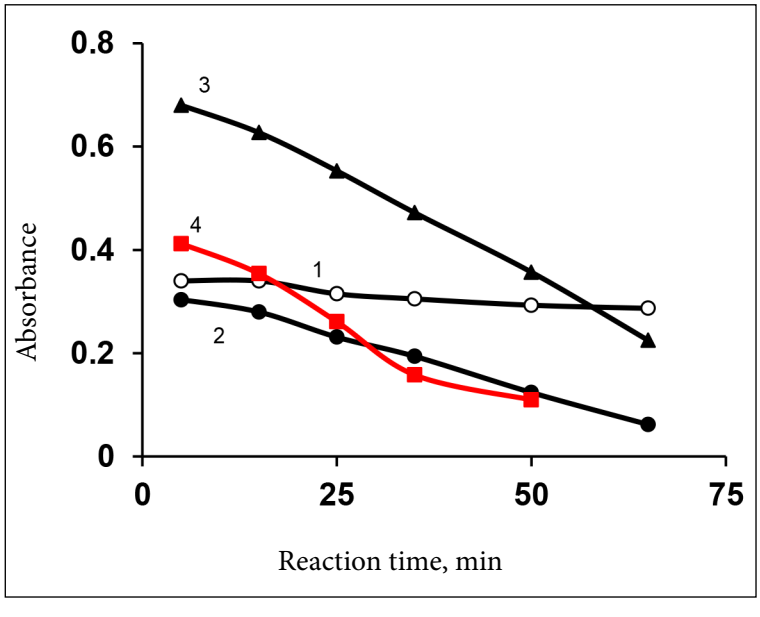

Fig. 6. Time dependent absorbance of the MO during the 65 min degradation reaction of mixtures of MO with H_2O_2 and CuO: (1) 5 mg/L MO, $T = 25$°C; (2) 5 mg/L MO, $T = 50$°C; (3) 10 mg/L MO, $T = 50$°C; (4) 5 mg/L MO, $T = 50$°C, green synthesized CuO

Conditions: 10 mL of MO solution, 1 mL H_2O_2, catalyst 3 mg CuO synthesized by sol–gel or green method.

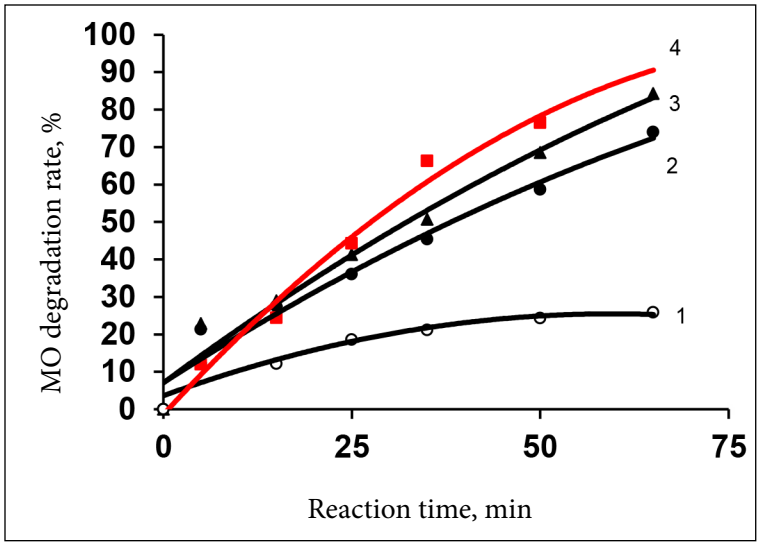

Fig. 7. Dependence of the degradation rate of MO dye in mixture with H_2O_2 and CuO on the MO dye concentration and temperature: (1) 5 mg/L MO, $T = 25$°C; (2) 10 mg/L MO, $T = 50$°C; (3) 5 mg/L MO, $T = 50$°C; (4) 5 mg/L MO, $T = 50$°C

Conditions: 10 mL of MO solution, 1 mL H_2O_2, catalyst 3 mg CuO synthesized using the following methods: (1, 2, 3) sol–gel method, (4) green synthesis.

green synthesized CuO exhibits a similar or even somewhat better activity at the same conditions when compared with CuO synthesized using the sol–gel method (Fig. 6, Curve 4 and Curve 2, respectively). The oxidative degradation rates of 5 mg/L MO at 50°C temperature after 65 min reaction time using the catalyst CuO synthesized by the sol–gel method or green synthesis were obtained as 76.2% and 86%, respectively.

The rate constant k of the MO degradation reaction was determined using the pseudo-first-order kinetic equation (Eq. 6) form presented in [24, 48, 49]:

$$\ln\frac{C_t}{C_0} \text{ or } \ln\left(\frac{A_t}{A_0}\right) = -kt\,. \tag{6}$$

Here k is the reaction rate constant, A_0 is the initial absorbance of the dye solution, and A_t is the absorbance of the dye solution after time t. The well-behaved linear fitting with the correlation factor R > 0.95 showed that the MO degradation proceeded in accordance with the pseudo-first-order kinetics. The rate constant k at two temperatures was calculated from the slope of the linear fitted lines. Whereas the rate constants calculated at two temperatures showed that when the reaction temperature was raised from 25°C to 50°C, the MO degradation reaction rate increased by 10.6 times (Table 2). Besides, the MO degradation reaction rate constant k obtained for the green synthesized CuO was higher than that using the CuO synthesized by the sol–gel method.

The values of thermodynamic parameters for the MO degradation reaction in the presence of

Table 2. **The rate constants for the catalytic oxidation of MO dye in the presence of H_2O_2 and catalyst CuO**

Methyl Orange concentration in solution, mg/L	T, °C	k, min^{-1}
CuO synthesized by sol–gel method		
5	25	0.0027
10	50	0.0291
5	50	0.0288
Green synthesized CuO		
5	50	0.0313

Conditions: 10 mL of 5 mg/L or 10 mg/L MO solution, 1 mL H_2O_2, 3 mg CuO

H_2O_2 and catalyst CuO nanoparticles synthesized by the sol–gel method were determined from the temperature dependence (298–323 K) of the rate constant k according to the Eyring equation that is a theoretical construct, based on the transition state model [24, 50]

$$\ln\left(\frac{k}{T}\right) = \ln\left(\frac{K_B}{h}\right) - \frac{\Delta H^{\#}}{RT} + \frac{\Delta S^{*}}{R}\,. \tag{7}$$

Here k is the rate constant of the reaction, K_B = Boltzmann's constant ($1.381 \cdot 10^{-23}$ J K^{-1}), T = absolute temperature in degrees Kelvin, h = Plank constant ($6.626 \cdot 10^{-34}$ J s), R = universal gas constant 8.314472, J K^{-1} mol^{-1}, $\Delta H^{\#}$ is the activation enthalpy (J mol^{-1}), and $\Delta S^{\#}$ is the activation entropy (J mol^{-1} K^{-1}).

The changes in the activation enthalpy ($\Delta H^{\#}$) and entropy ($\Delta S^{\#}$) were determined from the slope and intercept of the plot $\ln(k/T)$ versus $1/T$ of Eq. 6,

respectively. The free energy of activation (ΔG^0) was determined from Eq. 8:

$$\Delta G^{\#} = \Delta H^{\#} - T\Delta S^{\#}. \quad (8)$$

The values of the thermodynamic parameters obtained for the MO degradation reaction in the presence of the catalyst CuO synthesized by the sol–gel method were as follows: $\Delta G^{\#}$ = 79.18 kJ mol^{-1} (293 K) and $\Delta G^{\#}$=79.81 kJ mol^{-1} (323 K). The positive value of the activation enthalpy $\Delta H^{\#}$ = +73.03 kJ mol^{-1} indicated the endothermic nature of the MO degradation reaction. The obtained $\Delta H^{\#}$ value was higher than $\Delta S^{\#}$ suggesting that the degradation reaction is controlled by the enthalpy of activation. Meanwhile, the negative value of $\Delta S^{\#}$ = –0.021 kJ mol^{-1} K^{-1} reflects decreasing in the dispersal of energy at the catalyst CuO/solution interface during the reaction [51, 52].

CONCLUSIONS

CuO nanoparticles have been synthesized by sol–gel and green synthesis methods and characterized using XRD, SEM and UV-visible spectroscopy. The catalytic activity of CuO in the degradation reaction with H_2O_2 was proved using the organic dye Methyl Orange. Although the morphology of CuO depended on the synthesis method, at the same conditions the green synthesized CuO exhibits a similar catalytic activity as compared to the CuO synthesized using the sol–gel method. The oxidative degradation reaction rates of 5 mg/L MO at 50°C temperature after the 65 min reaction using the catalyst CuO synthesized by the sol–gel method or green synthesis were 76.2 and 86%, respectively.

The results indicate that the green synthesis of CuO nanoparticles is simple, minimizing the use of chemicals, and the prepared CuO could be a promising catalyst for the oxidative degradation of dye, especially used in medical procedures.

Received 11 July 2019
Accepted 10 September 2019

References

1. K. Hunger (ed.), *Industrial Dyes. Chemistry, Properties, Application*, Wiley-VCH, Weinheim (2003).
2. T. Poiger, S. D. Richardson, G. L. Baughman, *J. Chromatogr. A*, **886**, 259 (2000).
3. V. M. Correia, T. Stephenson, S. J. Judd, *Environ. Technol.*, **15**, 917 (1994).
4. S. F. Dubrow, G. D. Boardman, D. J. Michelsen, in: A. Reife, H. S. Freeman (eds.), *Environmental Chemistry of Dyes and Pigments*, J. Wiley, USA (1996).
5. P. Deka, R. C. Deka, P. Bharali, *New J. Chem.*, **40**, 348 (2016).
6. A. Banazadeh, H. Salimi, M. Khaleghi, S. Shafiei-Haghighi, *J. Environ. Chem. Eng.*, **4(2)**, 2178 (2016).
7. M. Horáková, Š. Klementová, P. Kříž, S. K. Balakrishna, P. Špatenka, O. Golovko, *Surf. Coat. Technol.*, **241**, 154 (2014).
8. I. Oller, S. Malato, J. A. Sanchez-Perez, *Sci. Total Environ.*, **409**, 4141 (2011).
9. J. L. Wang, L. J. Xu, *Crit. Rev. Env. Sci. Tech.*, **42(3)**, 251 (2012).
10. A. D. Bokare, W. Choi, *J. Hazard. Mater.*, **275**, 121 (2014).
11. F. J. Millero, R. L. Johnson, C. A. Vega, V. K. Sharma, S. Sotolongo, *J. Solution Chem.*, **21**, 1271 (1992).
12. J. I. Nieto-Juarez, K. Pierzchla, A. Sienkiewicz, T. Khon, *Environ. Sci. Technol.*, **44**, 3351 (2010).
13. H. Xu, G. Zhu, D. Zheng, C. Xi, X. Xu, X. Shen, *J. Colloid Interface Sci.*, **383**, 75 (2012).
14. Y. Zhong, T. Shi, Z. Liu, S. Cheng, Y. Huang, X. Tao, G. Liao, Z. Tang, *Sens. Actuators, B*, **236**, 326 (2016).
15. A. Wongrakpanich, I. A. Mudunkotuwa, S. M. Geary, et al., *Environ. Sci. Nano*, **3**, 365 (2016).
16. B. Andrews, S. Almahdali, K. James, S. Ly, K. N. Crowder, *Polyhedron*, **114**, 360 (2016).
17. B. Dutta, E. Kar, N. Bose, S. Mukherjee, *RSC Adv.*, **5**, 105422 (2015).
18. M. T. S. Chani, K. S. Karimov, S. B. Khan, A. M. Asiri, *Sens. Actuators, A*, **246**, 58 (2016).
19. J. Wang, Y. Liu, S. Wang, X. Guo, Y. Liu, *J. Mater. Chem. A*, **2**, 1224 (2014).
20. S. Shinde, H. Dhaygude, D. Y. Kim, et al., *J. Ind. Eng. Chem.*, **36**, 116 (2016).
21. G. Zhu, H. Xu, Y. Xiao, Y. Liu, A. Yuan, X. Shen, *ACS Appl. Mater. Interfaces*, **4**, 744 (2012).
22. Z. Yang, Y. Yang, X. Zhu, G. Chen, W. Zhang, *Ind. Eng. Chem. Res.*, **53(23)**, 9608 (2014).
23. H. Li, J. Liao, T. Zeng, *Catal. Commun.*, **46**, 169 (2014).
24. P. Deka, A. Hazarika, R. C. Deka, P. Bharali, *RSC Adv.*, **6**, 95292 (2016).
25. R. Kaushik, Ch. K. Ghoshb, Ch. K. Sarkara, *Mater. Res. Bull.*, **94**, 257 (2017).
26. M. R. Quirino, G. L. Lucena, J. A. Medeiros, I. M. Garcia dos Santos, M. J. Cunha de Oliveira, *Mater. Res.*, **21(6)**, e20180227 (2018).

27. C. Wang, Y. Ye, B. Tao, B. Geng, *Cryst. Eng. Comm.*, **14**, 3677 (2012).
28. L. M. Gilbertson, E. M. Albalghiti, Z. S. Fishman, et al., *Environ. Sci. Technol.*, **50**, 3975 (2016).
29. K. S. Joya, H. J. M. Groot, *ACS Catal.*, **6**, 1768 (2016).
30. J. Zhu, D. Li, H. Chen, X. Yang, L. Lu, X. Wang, *Mater. Lett.*, **58**, 3324 (2004).
31. R. V. Kumar, R. Elgamiel, Y. Diamant, A. Gedanken, J. Norwig, *Langmuir*, **17**, 1406 (2001).
32. A. A. Radhakrishnan, B. B. Beena, *Indian J. Adv. Chem. Sci.*, **2(2)**, 158 (2014).
33. M. S. Akhtar, J. Panwar, Y.-S. Yun, *ACS Sustain. Chem. Eng.*, **1(6)**, 591 (2013).
34. J. Singh, T. Dutta, K. H. Kim, M. Rawat, P. Samddar, P. Kumar, *J. Nanobiotechnol.*, **16**, 84 (2018).
35. J. Jeevanandam, Y. S. Chan, M. K. Danquah, *ChemBioEng Rev.*, **3(2)**, 55 (2016).
36. O. Zuasan, N. Hamima, Y. Samporab, *Mater. Lett.*, **123**, 156 (2014).
37. E. A. Terenteva, V. V. Apyari, S. G. Dmitrienko, Yu. A. Zolotov, *Spectrochim. Acta A*, **151**, 89 (2015).
38. M. Nasrollahzadeh, S. M. Sajadi, A. Rostami-Vartooni, S. M. Hussin, *J. Colloid Interface Sci.*, **466**, 113 (2016).
39. S. Hemmati, L. Mehrazin, M. K. Hekmati, M. Izadi, H. Veisi, *Mater. Chem. Phys.*, **214**, 527 (2018).
40. Sh. Prakash, N. Elavarasan, A. Venkatesan, K. Subashini, M. Sowndharya, V. Sujatha, *Adv. Powder Technol.*, **29**, 3315 (2018).
41. A. M. Awwad, B. A. Albiss, N. M. Salem, *SMU Med. J.*, **2(1)**, 91 (2015).
42. S. Gunalan, R. Sivaraj, R. Venckatesh, *Spectrochim. Acta, Part A*, **97**, 1140 (2012).
43. B. Kumar, K. Smita, L. Cumbal, A. Debut, Y. Angulo, *J. Saudi Chem. Soc.* **21**, 475 (2017).
44. M. Nasrollahzadeh, S. M. Sajadi, A. Rostami-Vartooni, S. M. Hussin, *J. Colloid Interface Sci.*, **459**, 183 (2015).
45. F. Duman, I. Ocsoy, F. O. Kup, *Mater. Sci. Eng. C*, **60**, 333 (2016).
46. S. Sanlı, C. Lunte, *Anal. Methods*, **6**, 3858 (2014).
47. J. Bandara, J. Kiwi, C. Pulgarin, et al., *Environ. Sci. Technol.*, **30(4)**, 1261 (1996).
48. M. N. Chong, B. Jin, C. W. K. Chow, C. P. Saint, *Chem. Eng. J.*, **152**, 158 (2009).
49. S. Lagergren, *Kungl. Svenska Vetenskapsakad. Handl.*, **24(4)**, 1 (1898).
50. A. Gemeay, *Dyes Pigm.*, **54**, 201 (2002).
51. R. C. Wilkins, *The Study of the Kinetics and Mechanism of Reactions of Transition Metal Complexe*s, p. 101, Allyn and Bacon, Boston, MA (1974).
52. P. Saha, Sh. Chowdhury, in: M. Tadashi (ed.), *Thermodynamics,* p. 349, InTex *(*2011).

D. Kaušpėdienė, E. Zubrytė, A. Gefenienė, M. Jovaišaitė, V. Gefenas, R. Binkienė, R. Ragauskas, A. Selskienė, V. Pakštas

ORGANINIO DAŽIKLIO OKSIDACINIO SKAIDYMO DALYVAUJANT H_2O_2 IR CuO NANODALELĖMS, GAUTOMS ZOLIŲ-GELIŲ IR ŽALIOSIOS SINTEZĖS METODAIS NAUDOJANT ŽIEDŲ (*Matricaria chamomilla*) EKSTRAKTĄ, EFEKTYVUMO PALYGINIMAS

S a n t r a u k a

CuO nanodalelės buvo susintetintos zolių-gelių ir žaliosios sintezės metodais naudojant žiedų (*Matricaria chamomilla*) ekstraktą. Sintetinių CuO nanodalelių RSD analizė aiškiai parodė kristalinę, monokliniņę jų prigimtį, kuri nepriklauso nuo sintezės metodo, o SEM atskleidė, kaip naudoti sintezės metodai paveikė CuO nanodalelių morfologiją. Tirta ir palyginta organinio dažiklio metiloranžo (MO) oksidacinio skaidymo kinetika, kai dalyvauja susintetintas katalizatorius CuO ir H_2O_2, atsižvelgiant į dažiklio koncentraciją, reakcijos laiką ir temperatūrą. CuO katalizinis aktyvumas buvo tiriamas matuojant MO dažiklio tirpalo, apdoroto CuO ir H_2O_2, UV-regimosios šviesos spindulių spektrą. Nustatyta, kad MO skilimo reakcijos kinetika vyksta pagal pseudo-pirmojo laipsnio reakcijos mechanizmą. Termodinaminiai tyrimai išryškino reakcijos endoterminę prigimtį ($\Delta H^{\#}$ = +73,03 kJ mol^{-1}) ir mažėjantį energijos išsibarstymą katalizatoriaus CuO tirpalo sąlyčio paviršiuje oksidacinio skaidymo reakcijos metu ($\Delta S^{\#}$ = –0,021 kJ mol^{-1} K^{-1}). Nepaisant sintezės būdo ir esant vienodoms skaidymo reakcijos sąlygoms CuO nanodalelės pasižymi panašiu kataliziniu aktyvumu. Be to, žalioji CuO nanodalelių sintezė yra paprasta, naudojanti mažiau cheminių medžiagų, o gautos CuO nanodalelės gali būti perspektyviu organinių dažiklių katalizatoriumi, ypač naudojamų medicininėse procedūrose, oksidaciniam skaidymui.